Spectral methods in gravity inversion: the geopotential field and its derivatives

Maria Zadro and Carla Braitenberg
Dipartimento di Scienze della Terra, Università di Trieste, Italy

Abstract
The 3D spectral analysis of the gravitational potential field for a given mass distribution is studied. The derived quantities, the gravitational force field and the gravity gradient tensor are computed in frequency space. As an example, the fields are theoretically and numerically evaluated for a right rectangular prism. The spectral approach finds several geophysical applications, as, *e.g.*, in inversion processes. Gravity inversion for deep seated masses, as for instance at Moho level, are treated with an iterative inversion process, in which the downward continuation is alternated with the classical calculation of the gravity field. The theory is applied to the inversion of the gravity data in the SE-Alps, regarding only the long-period field, generated by Moho undulations. The results are used for the evaluation of the equipotential lines, the gravity field, and the gravity gradient tensor in a vertical section of the Alpine crustal root.

Key words *gravity inversion – downward continuation – gravitational gradient tensor*

1. Introduction

For several decades spectral methods have been used to describe geopotential fields. Taking advantage of the great quantity of satellite data, both the gravitational and the magnetic fields are modelled at global scale by an expansion in spherical harmonics. At local and regional scale the spectral methodology can be developed in Cartesian coordinates, applying the Fourier transform. This offers a variety of interpretational possibilities scarcely used in practice. In the following we intend to point out some spectral characteristics of the geopotential fields, which follow directly from their physical mathematical 3D formulation. We regard two classes of problems: the surface and upper crust local inhomogeneities and the deeper horizontal discontinuities, as for example the Moho.

The more superficial local inhomogeneities may be in many cases approximated by geometrical objects of known shape, as the sphere, the right or inclined cylinder, or a right or inclined prism. The spectral approach gives some advantages particularly in the process of gravity inversion. The spectral problem has been approached in the past (*e.g.*, Odegard and Berg, 1965; Regan and Hinze, 1976) for particular geometric objects, giving a formulation of the spectrum of the gravity field which is the analytical evaluation of the spectrum of gravity distribution along a profile or in the horizontal plane (Bhattacharyya, 1966, 1967; Bhimasankaram *et al.*, 1977). This approach, however, masks the intrinsic relationship between properties of the spectrum (as positions of extremal values, characteristic decay curves) and the geometric dimensions, or the depth of the specific object, properties which are evident in the 3D-spectral evaluation of the potential field.

Mailing address: Prof. Maria Zadro, Dipartimento di Scienze della Terra, Università di Trieste, Via E. Weiss 1, 34100 Trieste, Italy; e-mail: zadro@univ.trieste.it

Regarding the deep-seated masses, the model of a single geometric object is generally not applicable, as the measured field is generated by the superposition of multiple anomalous masses, which can only poorly (at best) be separated. In this case it may be more convenient to model the system in terms of horizontal density discontinuity surfaces (Granser, 1987; Oldenburg, 1974; Parker, 1972). The task is then to determine the depth and undulation of the surfaces. A further problem which can be tackled with the 3D-spectral approach is that of the effect of self-gravitation. As will be shown further on, the presence of an anomalous mass in the crust influences the geopotential field, as well as the gravity field and the stress field throughout the surrounding crust. In the present paper we evaluate the variation in the potential field, in gravity, and its derivatives due to the presence of the crustal roots in the Southern Alps.

2. The 3D spectrum of gravitational fields

The Newtonian potential field U produced at a point P by a density mass distribution $\rho(P_0)$ with (P_0) inside the volume (V) can be considered as a convolution product (Zadro, 1984, 1986):

$$U(P) = G\frac{1}{r} * \rho(P_0) \qquad (2.1)$$

with G the gravitational constant, $\rho(P_0) = 0$ for (P_0) outside (V), and $r = |P - P_0|$. $(1/r)$ is the Green function of the process.

It follows that the Fourier Transform (FT) of the potential field is given by:

$$\mathrm{FT}[U(P)] = G\,\mathrm{FT}[1/r]\,\mathrm{FT}[\rho(P)], \quad (2.2)$$

where $\mathrm{FT}[1/r] = \dfrac{1}{\pi\sigma^2}$ (Sneddon, 1951), with

$$\sigma^2 = \alpha^2 + \beta^2 + \gamma^2;$$

α, β, γ being the wavenumbers along the x, y, z coordinates, respectively. The relationship (2.2) holds in the entire space.

The Newtonian gravitational forces acting along whatever direction $\vec{n}$ in the wavenumber space are:

$$\mathrm{FT}[\vec{\nabla}U\,\vec{n}] = -2\pi i v\,\mathrm{FT}[U]$$
$$\text{with} \quad v = \alpha n_x + \beta n_y + \gamma n_z. \qquad (2.3)$$

In gravity anomaly studies $\vec{n}$ is generally vertical so that

$$\mathrm{FT}[\vec{\nabla}U\,\vec{e}_3] = -2\pi i \gamma \mathrm{FT}[U], \qquad (2.3')$$

whereas, for the horizontal components we have (*e.g.*, along the x direction):

$$\mathrm{FT}[\vec{\nabla}U\,\vec{e}_1] = -2\pi i \alpha \mathrm{FT}[U]. \qquad (2.3'')$$

Here $\vec{e}_1$ and $\vec{e}_3$ are the unitary vectors along α and γ, respectively.

The gravitational gradient tensor can also be easily computed for a self-gravitating body, inasmuch as the tensor matrix τ_{ij} is given in the α, β, γ space by

$$\mathrm{FT}(\tau_{ij}) = -4\pi^2\alpha\beta\,\mathrm{FT}[U] \qquad (2.4)$$

and analogously for the other matrix elements.

The study of the gravitational gradient tensor can be of interest in gradiometry and in several geodynamical processes where structures with large density variations collide.

3. Geophysical applications

In the previous section the spectral properties of the potential field, the gravitational forces and the gravitational gradient tensor were given. The anti- Fourier transform (FT^{-1}) of the above functions allows us to obtain the following quantities in the entire 3D space, including the inside of the gravitating body:

a) Equipotential surfaces, which can give information, *e.g.*, on the geoidal undulations.

b) Gravitational forces, which have application in the solution of gravity anomaly inversion problems. Both surface perturbing bodies and deep layered media (isostatic effects and Moho undulations) can be treated.

c) The tensor of the second derivatives of the potential, useful in gradiometry as well as in the evaluation of the Newtonian stress tensor due to intruded anomalous masses.

Particular techniques can sometimes be applied in geophysical problems in order to reduce the 3D spectrum to a 2D one. Three significant cases are mentioned below.

In the analysis of gravity anomaly data along profiles crossing orthogonally (*e.g.*, aligned along x) parallel structural lineaments (aligned along y), the perturbing bodies can be assumed of infinite extension. The spectrum reduces to a 2D spectrum, function of α and γ, as following (2.2):

$$\mathrm{FT}\,[U(P)] = G\,\mathrm{FT}\,[1/r]\,\mathrm{FT}\,[\rho(P)]\,\delta(\beta) \quad (3.1)$$

with $\delta(\beta)$ the δ of Dirac.

A second case regards the comparison between the 2D spectrum (therefore function of α and β) of a surface distribution of observed gravity anomalies and the corresponding theoretical one calculated for a 3D model. The latter is given by the $\mathrm{FT}^{-1}_{\gamma,\, z = z_0}$ of the 3D spectrum (computed according to (2.3′) with the antitransform carried out for the γ variable only and for an assigned z_0 surface reference level. Of course, the observational data can as well be compared with the theoretical ones computed through the 3D FT^{-1}, where the theoretical anomalies are given at all sampled z levels, thus allowing a check of the assumed depths and shapes of the modelled perturbing bodies.

A third particularly interesting case is the one concerning deep horizontal inhomogeneous layers or discontinuities like the Moho. In this case the perturbing mass is simulated by a surface mass distribution (see *e.g.*, Tsuboj, 1983) and the process is known as the «gravity continuation law». It results that, for a gravity anomaly (Δg) at the surface ($z = 0$) induced by a surface mass distribution $\sigma(x, y)$ located at a depth (z_0),

$$\mathrm{FT}\,[\Delta g] = 2\pi G\,\mathrm{FT}\,[\sigma]\, e^{-2\pi z_0 (\alpha^2 + \beta^2)^{\frac{1}{2}}} \quad (3.2)$$

and

$$\sigma = \frac{1}{2\pi G}\,\mathrm{FT}^{-1}\left[\mathrm{FT}\,[\Delta g]\, e^{2\pi z_0 (\alpha^2 + \beta^2)^{\frac{1}{2}}}\right]. \quad (3.2')$$

For an assigned depth (z_0), $\sigma(x, y)$ can be calculated, and by assuming a known value for the density contrast ρ_0 (the density contrast between crust and mantle in the case of the Moho), the undulation amplitude $h(x, y)$ is given by

$$h(x, y) = \sigma(x, y)/\rho_0. \quad (3.3)$$

The above technique presents two serious problems. The first is the amplification of high wave number energies, especially for great depth (z_0) values, caused by noise and surface gravity perturbations of no interest. This effect can be avoided through suitable low-pass filtering (Santero *et al.*, 1988). The second problem is the assumption of a surface mass distribution instead of a 3D mass distribution. In cases of deep crustal roots (Moho discontinuity) the solution can be improved by means of an iterative process (Parker, 1972; Braitenberg *et al.*, 1997) as shown below.

4. The spectrum of a right rectangular prism

The numerical evaluation of the spectral field of the gravitational potential or the derived quantities as the gravitational forces and the gravitational gradient tensor, requires the 3D FT of the density distribution. Generally, the mass distribution may be modelled by a series of right vertical prisms of constant density. The spectrum of the total mass distribution is then equal to the sum of the spectral distributions of the single prisms.

Given a right rectangular prism of sides A, B, C aligned with the x, y, z axes of the reference system, respectively, and centred with its centre of mass in the origin, the Fourier spectrum is given by

$$\mathrm{FT}\,[\rho] = \rho_0\ \mathrm{dif}\ (\alpha, A)\ \mathrm{dif}\ (\beta, B)\ \mathrm{dif}\ (\gamma, C) \quad (4.1)$$

with the density of the prism (ρ_0) and the sine-function dif $(\lambda, L) = \sin(\pi\lambda L)/\pi\lambda$.

In the far field it is sufficient to approximate the mass distribution by point-masses located in the centre of mass of elementary cubes. For one single point mass the density distribution is defined by

$$\rho(x, y, z) = \rho_0\, \delta(x)\, \delta(y)\, \delta(z),$$

and the FT is equal to

$$\mathrm{FT}(\rho) = \rho_0.$$

Applying the transformation law of the FT for lateral shift gives the FT for the density distribution centred at the point (x_0, y_0, z_0):

$$\mathrm{FT}[\rho(x-x_0,\ y-y_0,\ z-z_0)] =$$

$$= \mathrm{FT}[\rho(x, y, z)]\, e^{-i2\pi(\alpha x_0 + \beta y_0 + \gamma z_0)}. \qquad (4.1')$$

Other transformation laws (Arsac, 1961, pp. 116-120) can be applied in the computation of the FT $[\rho]$. The most important one concerns the rotation: a rotation Ω in the x, y, z space results in a rotation Ω in the α, β, γ space, so that inclined prisms (*e.g.*, simulating inclined faults) can also be calculated from (4.1) by rotating the α, β, γ coordinate system.

From the total mass distribution spectrum all the other spectral matrices regarding the Newtonian potential and its derivatives can be easily obtained following the expressions (2.2), (2.3) and (2.4).

In the above numerical procedure both sampling and Nyquist frequencies have to be carefully chosen in order to avoid truncation and aliasing effects. It is well known that sampling in the α, β, γ space corresponds to the truncation (and repetition) in the x, y, z space and viceversa. Moreover border effects strongly appear in the FT^{-1} process, as a consequence of the infinite repetitions in the x, y, z space of the gravitating masses according to the FT law. This implies that the spectral resolution must be chosen small enough, or equivalent by the x, y, z space extensive enough so as to shift the repetition effects beyond the zone of interest. Regarding the position of the Nyquist frequencies (inversely dependent on the space sampling $\Delta x, \Delta y, \Delta z$), the problem is less critical: the mass distribution, the Newtonian potential and its derivatives appear as «transient» phenomena, to which the energies are concentrated at low frequencies with rapidly decreasing spectra. Nevertheless, in order to avoid aliasing effects the computed spectral values should be almost evanescent at Nyquist frequencies.

A particular case of geophysical interest is that of a mass distribution infinitely extended along a horizontal direction. As already stated above, this case reduces to 2D: in (4.1) dif (β, B) simplifies to $\delta(\beta)$ for a prism infinite in the y direction, so that all the above computational considerations are still valid. In this simplified case of course we have to deal with 2D repetition spectra.

5. Moho undulations – the SE-Alps as an example

Deep seated horizontal density contrasts can be treated applying the downward continuation, as defined in (3.2). A problem arises when interpreting the variation of surface density as a vertical undulation of the discontinuity surface. It can be shown that the gravity field (Parker, 1972) produced by the undulating surface deviates considerably from the gravity field produced by the equivalent flat sheet with varying surface density. A two-step iterative procedure in which the undulation is corrected at each iteration was developed in Braitenberg *et al.* (1997). The two iteration steps are explained below, where the variable iter starts from iter = 1, increasing at each iteration step by 1.

Starting values are the sampled Bouguer gravity $b(i, j)$ $(i = 1, n;\ j = 1, m)$ data placed on a regular $n \times m$ grid. Two free parameters must be set, which are the mean Moho depth (d) and the contrast $\Delta\rho$ between crust and mantle densities (ρ_c) and (ρ_m). The Bouguer anomalies must be low pass filtered, in order to eliminate short wavelength variations not related to deep structures. Furthermore the process of downward continuation must be limited in frequency, as it becomes unstable at high frequencies.

In the first step the undulation of the crust-mantle boundary $r_{\text{iter}}(i, j)$ is calculated by applying the expressions (3.2′) and (3.3) to this particular case, obtaining:

$$h_{\text{iter}}(i, j) = \text{FT}^{-1}\left[\text{FT}\left[\delta g_{\text{iter}-1}(k, l)\right] e^{-2\pi s d}\right] \frac{1}{2\pi G \Delta\rho}$$

for $i = 1, n$; $j = 1, m$ and $k = 1, n$; $l = 1, m$

$$\text{with} \quad s = \sqrt{\left(k/n\right)^2 + \left(1/m\right)^2} \qquad (5.1)$$

$$r_{\text{iter}}(i, j) = r_{\text{iter}-1}(i, j) + h_{\text{iter}}(i, j)$$

$\delta g_{\text{iter}-1}$ is the gravity residual between observed and model Bouguer gravity data (see next step). For the starting iteration (iter = 1) it is set equal to the observed gravity $\delta g_0(i, j) = b(i, j)$; h_{iter} is the calculated undulation. At the first iteration (iter = 1) the Moho is assumed flat: $r_0(i, j) = d$.

In the second step the Moho undulation is approximated by a series of vertical rectangular prisms, of sides A and B, and the gravity field is calculated at geoidal level by classical methodology (Nagy, 1966). The residual gravity δg_{iter} is defined as the difference between the observed and modelled gravity effect.

The above two steps are then repeated iteratively, obtaining each time a correction to the undulation of the Moho surface, until the gravity residual has reached an acceptable value, or equivalently, the corrections to the Moho surface are insignificant.

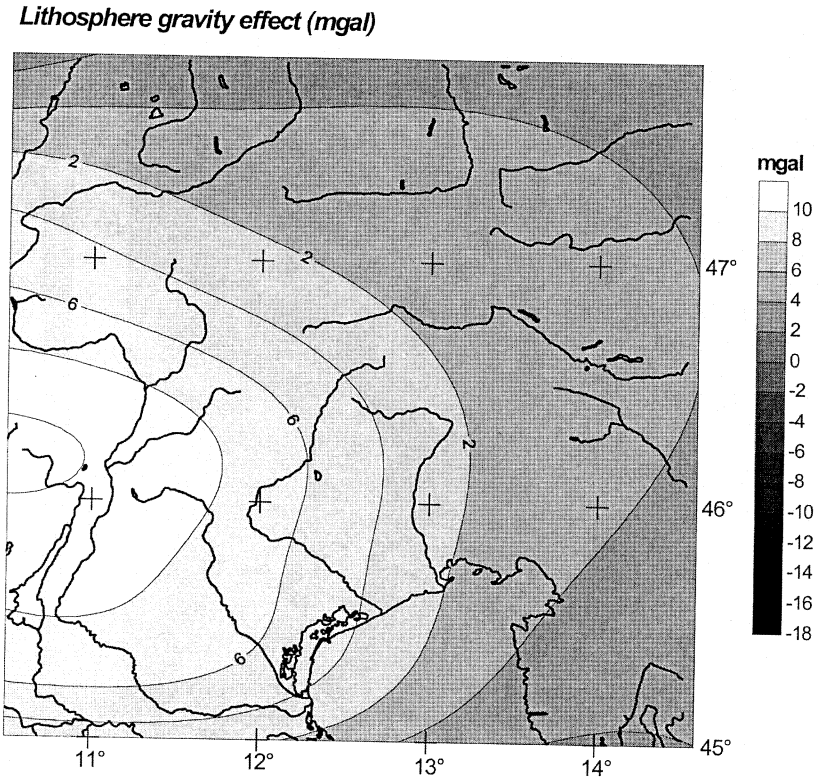

Fig. 1. Gravity effect (mgal) of the lithosphere roots in the studied area. Contour interval 2 mgal.

We apply the above iteration scheme to evaluate the Moho undulations in the SE-Alps. Complete Bouguer gravity data were furnished by BGI (Bureau Gravimetrique International) and integrated in the SE part of the studied area (Slovenia and part of the Adriatic Sea) with data of the 0.5° grid distributed by Prof. I. Marson, Trieste. The complete data set (10-15°E, 44-48°N) was gridded (inverse square distance) on a 5×5 km grid obtaining a 108×128 point grid. The analyses were done on this larger grid, whereas the final results are considered in a reduced (90×90) grid, in order to eliminate border effects. As the inversion regards exclusively the Moho undulation, the Bouguer data were corrected for the gravity effect produced by the lithosphere thickening beneath the Alpine chain. The lithosphere was modelled by a series of prisms (density contrast 0.03 g/cm^3) in the geographical area 44-50°N and 7-15°E at a resolution of 0.5°, according to the physical properties of the asthenosphere-lithosphere system given in Suhadolc *et al.* (1990). The lithosphere gravity effect is shown in fig. 1; the Bouguer data, corrected for the lithosphere gravity effect, are shown in fig. 2.

Table I shows the root-mean square of the residual anomalies (RMS) in mgal and the minimum (R_{min}) and maximum (R_{max}) Moho depths in km obtained in successive iterations. A decrease in the RMS at each iteration can be observed. We regard three iteration steps as sufficient, as only a very modest correction to

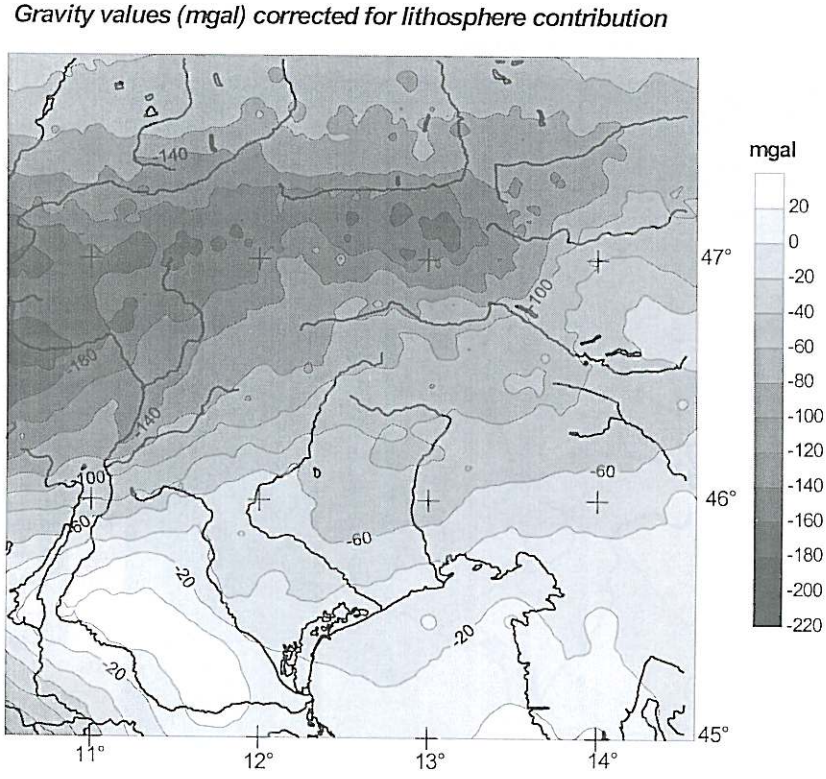

Fig. 2. Bouguer gravity map of North-Eastern Italy (BGI), corrected for the gravity effect of the lithosphere roots. Contour interval 10 mgal.

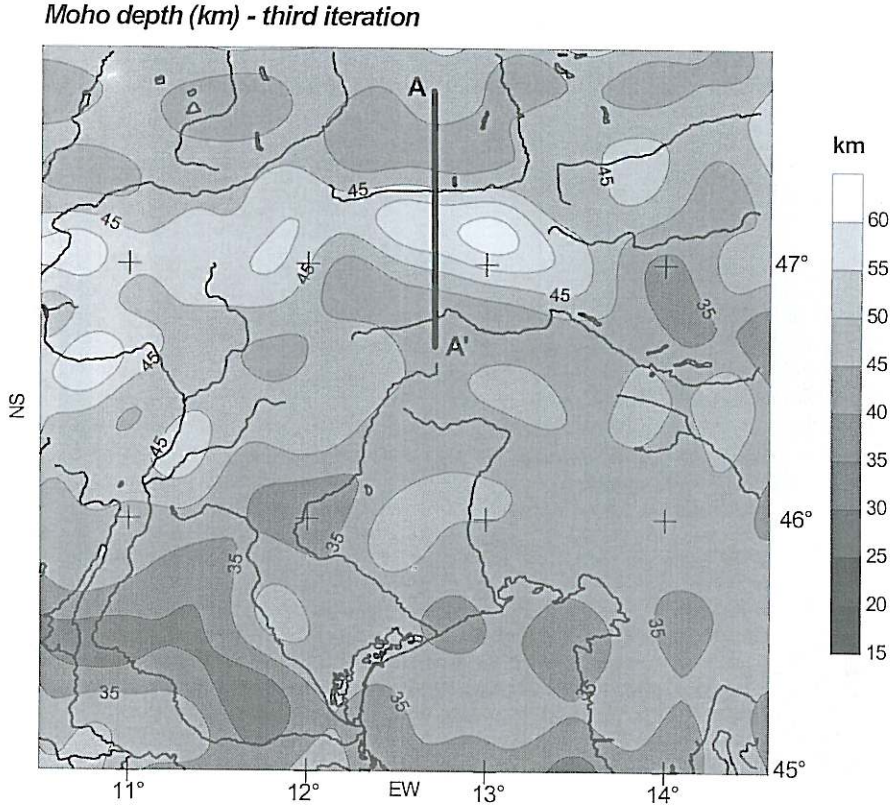

Fig. 3. Moho depths (km) in the SE-Alps obtained from the iterative inversion algorithm of the Bouguer gravity data, corrected for the lithosphere effect. Contour interval 5 km. The profile AA′ refers to the vertical section along which we evaluate the gravitational potential, forces and stresses.

Table I. Iterative inversion of gravity data in the SE Alps. For iteration steps 1-5 the extremal values of the Moho undulation (R_{min} and R_{max}) and the standard deviation of the gravity residual are tabulated.

Iteration step	R_{min} (km)	R_{max} (km)	Gravity residual (mgal)
1	29.5	49.2	10.2
2	27.5	54.1	5.8
3	26.2	57.4	4.7
4	25.2	60.0	4.3
5	24.5	62.2	4.1

the root is obtained at further steps. The Moho undulation at the third iteration is shown in fig. 3. The most prominent features are the pronounced deepening below the Alpine arc, the Moho high in the SW area of study (Vicenza high), and the shallowing of Moho to a depth of 35 km below the Adriatic sea. The 2D results are in excellent agreement with the map of Moho depth obtained unifying different DSS-profiles available in the area (Slejko *et al.*, 1987, p. 26). The modelled gravity at the third iteration is shown in fig. 4. The modelled values reconstruct the observed field well, as regards the long period features. The short period components in the observed field are due to the presence of superficial inhomogeneities, not considered in the analysis.

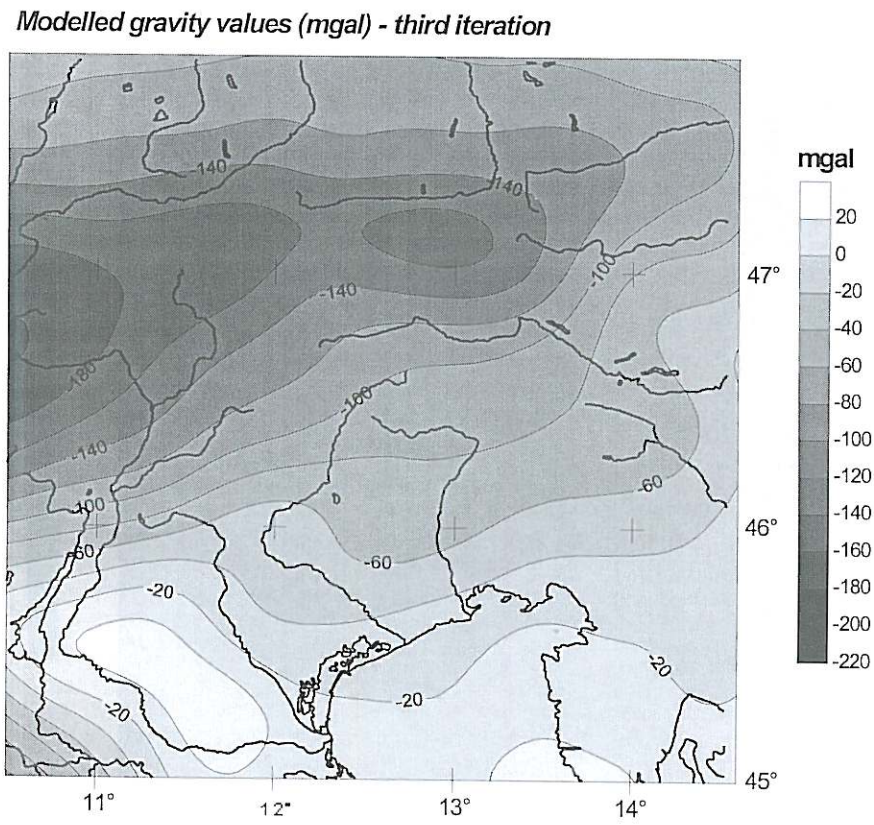

Fig. 4. Modelled gravity values after three iterations. Contour interval 10 mgal.

6. The gravitational potential, forces and gradient tensor across a section of the Alpine crustal roots

We proceed to evaluate the equipotential lines, the gravity values, and the gravitational gradient tensor field in a vertical section crossing the E-Alps, taking advantage of the spectral properties of the gravitational potential field. As shown above, the crustal root may be approximated by a series of right rectangular prisms. It is therefore convenient to consider at first the fields generated by a single prism.

From (4.1) and (2.2) we may construct the FT of the potential field of a single prism of width A and length L (infinite in one horizontal direction), centred in the point x_0, z_0 by

$$\mathrm{FT}[U(P)] = G\rho \frac{1}{\pi\sigma^2} \frac{\sin \pi\alpha A}{\pi\alpha} \frac{\sin \pi\gamma L}{\pi\gamma} e^{-i2\pi(\alpha x_0 + \gamma z_0)} \tag{6.1}$$

where

$$\sigma^2 = \alpha^2 + \gamma^2.$$

The potential is obtained from the anti transform of expression (6.1), the gravitational forces and the components of the gravitational gradient tensor τ_{xx}, τ_{zz}, τ_{xz} from the anti transform of the expressions (2.3′) and (2.4), respectively.

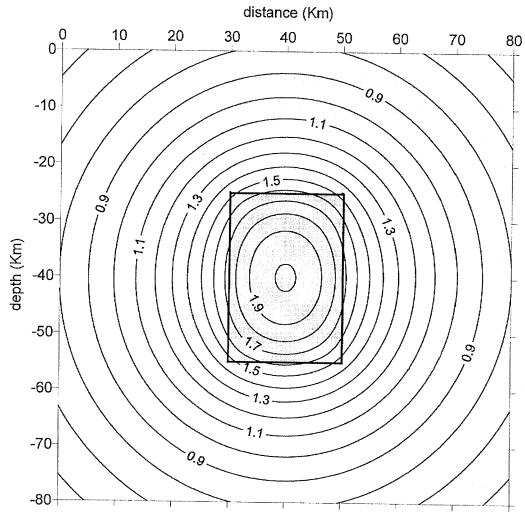

Fig. 5. Vertical section in the x-z plane crossing the rectangular right vertical prism of sides 20 km × 30 km. Isolines of the potential field (10^6 cm^2/s^2).

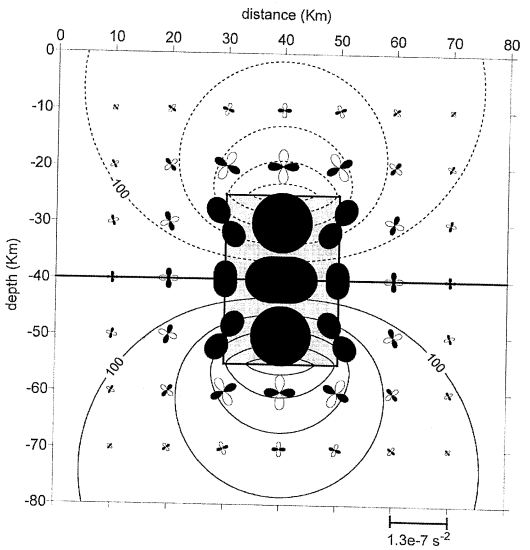

Fig. 6. Vertical section in the x-z plane crossing the rectangular right vertical prism of sides 20 km × 30 km. Isolines of the vertical gravity force component (100 mgal contour interval) and directional variation of the negative (black filled) and positive (white) components of the gravitational gradient tensor (10^{-7} 1/s^2).

The isolines of the potential (10^6 cm^2/s^2) in the (x, z)-plane are graphed in fig. 5. Figure 6 shows the isolines of the vertical force component (cm/s^2). The tensor components in the plane are represented at single points in terms of the directional variation of the negative (blackened) and positive (whitened) tensor components (10^{-7} 1/s^2). The graphical representation is analogous to that used for the plane stress tensor. The forces and tensor components are for a unitary mass. The position of the prism (20 km width, 30 km length) is drawn in the figure; the prism is infinite in the y-direction, orthogonal to the sheet-plane. The density of the prism is $\rho = 1$ g/cm^3. The fields were calculated on a 280×280 point grid, whereas we display a subgrid of 80×80. Considering the spatial Nyquist-frequencies, the maximum sampling is $dx = 10$ km, $dz = 15$ km for this particular prism. We used a more convenient value $dx = dz = 1$ km. For graphic convenience an arbitrary additive constant was chosen for the potential values, equal to the minimum potential value over the grid. The isolines of the vertical force resemble the dipole field: the vertical force is specular with respect to the horizontal plane passing through the centre of mass of the prism, and pointing downwards above the prism, and upwards below it. Internally to the prism the compressive component of the gravitational gradient tensor prevails above the extensional component.

We may now apply the above procedure for the series of prisms approximating the section AA′ (fig. 3) of the Alpine crustal root, 100 km long. In order to obtain a greater discretization the results for the Moho undulation were integrated with those obtained in a previous 2.5D inversion (Braitenberg *et al.*, 1997). The latter had been done with a sampling of 1 km, and with prisms of 4 km width. The prisms approximating the root extend infinitely in a horizontal direction orthogonal to the profile. The density of the prisms is set equal to $\Delta\rho = -0.53$ g/cm^2. In this case the fields were calculated on a 500×500 grid, with a sampling of $dx = dy = 1$ km. We display a subgrid of 100×90, excluding the border effects. Analogously to the graphs regarding the single prism, fig. 7, gives the equipotential lines and fig. 8 the isolines

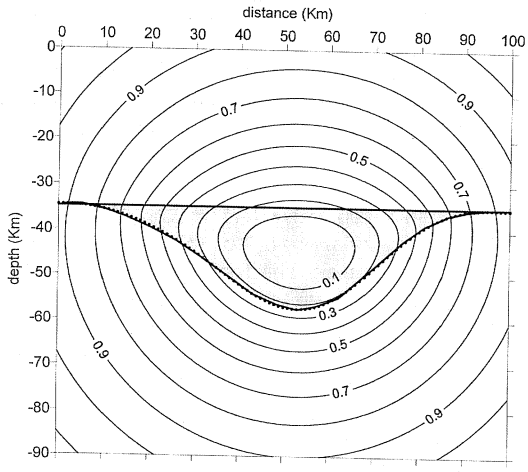

Fig. 7. Vertical section in the x-z plane crossing the Alpine crustal root along profile AA′ (fig. 2). Isolines of the potential field (10^6 cm^2/s^2).

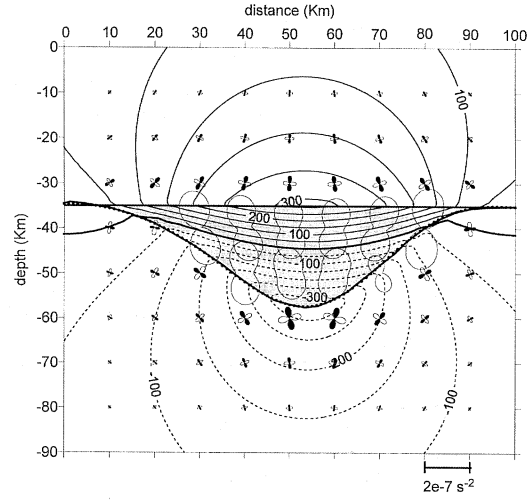

Fig. 8. Vertical section in the x-z plane crossing the Alpine crustal root along profile AA′ (fig. 2). Isolines of the vertical gravity force component (mgal) and directional variation of the negative (black filled) and positive (white) components of the gravitational gradient tensor (10^{-7} 1/s^2).

of the vertical force component together with the graphical representation of the gravitational gradient tensor. Due to the negative density, the potential values decrease towards the negative mass anomaly, the contrary of what is observed for the single prism of positive density. Considering the potential variations at the surface (z = 0) and adopting a normal gravity value of 981 gal, the deepening in geoidal height from a position above the center of the root and at km-mark zero amounts to about 2.5 m. The crustal root exerts a considerable distortion of the regular gravity field, as can be seen from the isolines of the vertical force component (fig. 8). Internally to the root the extensional component of the gravitational gradient tensor prevails above the compressional component. Regarding the magnitude of the gravitational gradient induced by the moon, which causes the tidal deformations and which can be estimated to the value of about 1.8 10^{-13} 1/s^2 (Falk and Ruppel, 1983), the gravitational gradient generated by the Alpine crustal root in its immediate neighbourhood is far greater: just above the upper border of the root the positive gradient component amounts to 8 10^{-7} 1/s^2.

7. Conclusions

The spectral approach can be a useful tool in the understanding and interpretation of several gravimetric problems concerning geodesy and geophysics. In the present paper the FT methodology is applied, which is defined for Cartesian coordinates. This implies that regional areas are considered, in which the Earth's curvature can be neglected. Large memory storage is needed, but this is not a problem with present computers.

The 2D downward continuation law is applied in the inversion problem treated in section 5. It is shown how the continuation law itself, combined in iterations with the classical computation of the gravitational field can give successful results, thus overcoming the too simple approximation of a horizontal deep discontinuity with a plane mass distribution.

In section 6 the FT methodology presented in section 1 is applied to an elementary body, and thereafter to an actual geodynamical case regarding a vertical section across the E Alpine chain.

The above process is particularly relevant in inversion and interpretation problems regarding geodesy, geodynamics, and geophysical prospections, inasmuch as the values of the potential field as well as that of its first and second derivatives in the whole selected grid can be obtained very quickly (the FT computer time is almost negligeable).

In some cases of gravimetric inversion, the perturbing mass may be known, but its depth is to be determined. The spectral method allows gravity values to be obtained in a vertical section, and thus at various levels above the perturbing mass. The depth of the mass can thus be determined by comparison of the observed values with the computed ones.

In geodetic problems the method allows to compute, as in the example of fig. 7, the geoidal undulations caused by large deep discontinuities as well as the vertical and horizontal variations of the gravity vector. As far as other geodetic interests are concerned, we can also mention the great importance of the tensor given by the second derivatives of the potential in the Marussian Intrinsic Geodesy and in gradiometry. Moreover, the above tensor can be usefully applied in geodynamic problems in order to evaluate the stress contribution due to the Newtonian effects of nearby perturbing masses of high density contrast.

Acknowledgements

Thanks are due to Dr. Rosanna Drigo for her valuable help in the numerical and graphical data treatment. The work was done with the financial contributions MURST 40%95-96-Zadro, CNR 95.00339.CT05 Zadro, 60%-96 Zadro, and CNR 96.00289CT05 Braitenberg.

REFERENCES

ARSAC, J. (1961): *Transformation de Fourier et Theorie des Dstributions* (Dunod, Paris) pp. 116-120.

BHATTACHARYYA, B.K. (1966): Continuous spectrum of the total-magnetic-field anomaly due to a rectangular prismatic body, *Geophysics*, **31**, 97-121.

BHATTACHARYYA, B.K. (1967): Some general properties of potential fields in space and frequency domain: a review, *Geoexplor.*, **5**, 127-143.

BHIMASANKARAM, V.L.S., R. NAGENDRA and S.V. SESHAGIRI RAO (1977): Interpretation of gravity anomalies due to finite inclined dykes using Fourier transformation, *Geophysics*, **42**, 51-59.

BRAITENBERG, C., F. PETTENATI and M. ZADRO (1997): Spectral and classical methods in the evaluation of moho undulations from gravity data: the NE Italian Alps and isostasy, *J. Geodyn.*, **23**, 5-22.

FALK, G. and W. RUPPEL (1983): *Mechanik, Relativität, Gravitation: die Physik des Naturwissenschaftlers* (Springer Verlag, Heidelberg), 1-445.

GRANSER, H. (1987): Nonlinear inversion of gravity data using the Schmidt-Lichtenein approach, *Geophysics*, **52**, 88-93.

NAGY, D. (1966): The gravitational attraction of a right rectangular prism, *Geophysics*, **30**, 362-371.

ODEGARD, M.E. and J.W. BERG (1965): Gravity interpretation using the Fourier integral, *Geophysics*, **30**, 424-438.

OLDENBURG, D.W. (1974): The inversion and interpretation of gravity anomalies, *Geophysics*, **39**, 424-438.

PARKER, R.L. (1972): The rapid calculation of potential anomalies, *Geophys. J. R. Astron. Soc.*, **31**, 447-455.

REGAN, R.D. and W.J. HINZE (1976): The effect of finite data length in the spectral analysis of ideal gravity anomalies, *Geophysics.*, **41**, 44-55.

SNEDDON, I.N. (1951): *Fourier Transforms* (McGaw Hill, New York), p. 514.

SANTERO, P., M. ZADRO, D. BLITZKOW and N.C. DE SÀ (1988): Gravimetric analysis of the Goiania flexure, Northern Paranà Basin, in *The Mesozoic Flood Volcanism of the Paranà Basin – Petrogenetic and Geophysical Aspects*, edited by E.M. PICCIRILLO and A.J. MELLI, Universidade de Sao Paolo, Instituto Astronomico e Geofisico, 257-269.

SLEJKO, D., G.B. CARULLI, F. CARRARO, D. CASTALDINI, A. CAVALLIN, C. DOGLIONI, V. ILICETO, R. NICOLICH, A. REBEZ, E. SEMENZA, A. ZANFERRARI and C. ZANOLLA (1987): Modello sismotettonico dell'Italia Nord-Orientale, *Rend. GNDT*, CNR, Roma, **1**, 1-82.

SUHADOLC, P., G.F. PANZA and S. MUELLER (1990): Physical properties of the lithosphere-asthenosphere system in Europe, *Tectonophysics*, **176**, 123-135.

TSUBOJ, C. (1983): *Gravity* (George Allen & Unwin, Boston), 1-254.

ZADRO, M. (1984): Spectral properties of the Newtonian potential field and their application in the interpretation of the gravity anomalies, *Geophys. J. R. Astron. Soc.*, **79**, 489-494.

ZADRO, M. (1986): Spectral images of the gravitational field, *Manuscripta Geodaetica*, **11**, 207-213.